# Cardiac Specific Overexpression of Adenylyl Cyclase 8 Reprograms the Mouse Sinoatrial Node Transcriptome

**Jia-Hua Qu[1,2], Kirill V. Tarasov[1], Khalid Chakir[1], and Edward G. Lakatta[1,*]**

1. **Laboratory of Cardiovascular Science, Intramural Research Program, National Institute on Aging, National Institutes of Health, Baltimore, MD 21224, USA.**
2. **Department of Host Microbe Interactions, St. Jude Children's Research Hospital, Memphis, TN 38105, USA.**

**Address correspondence to:**

**Dr. Edward G. Lakatta***

**Laboratory of Cardiovascular Science**

**Intramural Research Program**

**National Institute on Aging**

**National Institutes of Health**

**251 Bayview Boulevard**

**Suite 100**

**Baltimore, MD 21224**

**USA.**

**Tel: +1 410-558-8202**

**lakattae@grc.nia.nih.gov**

## Abstract

A coupled-clock system intrinsic to sinoatrial node (SAN) pacemaker cells that regulates the rate and rhythm of spontaneous action potential firing, is activated by $Ca^{2+}$/calmodulin-stimulated Adenylyl Cyclase (AC) types 8 and 1. Our previous work in mice with cardiac specific overexpression of human AC8 gene (TGAC8) discovered that compared to its wild-type (WT) littermates, the heart rate (HR) of TGAC8 is elevated (by about 30%, 24 hours a day, 7days a week), and that the TGAC8 heart rhythm is markedly coherent, i.e., the HR Variability (HRV) lacks complexity, similar to that associated with aging or cardiac pathology. Reprogramming of molecular mechanisms, particularly SAN transcriptomic regulation that underlies the remarkable chronic shift in HR and HRV, however, has not been delineated. We conducted deep RNA sequencing (RNA-seq) in TGAC8 and WT SANs, using Mm10plus with human ADCY8 DNA sequence as the reference genome. Utilizing multiple bioinformatic techniques, we not only profiled the expression of marker genes related to SAN functions and AC-cAMP-PKA signaling, but also discovered negatively enriched hub pathways that differed in TGAC8 vs. WT, the top three being OXPHOS, ribosome, and cardiac muscle contraction. In contrast, signaling pathways related to inositol phosphate and its metabolism were positively enriched in TGAC8. Further, we identified two transcription regulators, KDM5A and PPARGC1A, that mediate effects of TGAC8 on ribosome and mitochondria. In summary, reprogrammed transcriptional regulation increases the HR of TGAC8 at the cost of impairment of other SAN cell functions, i.e., altered ribosome and inositol phosphate signaling and its crosstalk with mitochondria. Because these cell signaling alterations are associated with cardiac aging and age-associated CVDs, the TGAC8 mouse appears to be

an ideal model in which to probe for potential therapeutic targets for cardiac aging and age-associated CVDs.

## Key Words

Sinoatrial Node, Adenylyl Cyclase 8, Transcriptome, Coupled-Clock System, Ribosome, Mitochondria, Inositol Phosphate

## Introduction

According to the report from World Health Organization (https://www.who.int/cardiovascular_diseases/about_cvd/en/), cardiovascular diseases (CVDs) are the leading cause of death globally. The decline of cardiac performance in CVDs may result from an impaired contractile function[1,2]. As one of the most important regulators of contraction, cAMP is catalyzed by adenylyl cyclases (ACs) upon activation by catecholamines binding to β-adrenergic receptors (β-ARs), and degraded by phosphodiesterases (PDEs)[3]. The activated ACs-cAMP-PKA signaling pathway promotes the phosphorylation of key proteins, contributing to strong positive inotropic, lusitropic, and chronotropic responses[3]. Therefore, the desensitization of the β-adrenergic signaling pathway, with the down-regulation of β1-ARs and ACs, disrupts the excitation-contraction coupling, resulting in CVDs[4].

Contrary to two main AC isoforms expressed in the heart, AC5 and AC6, two additional isoforms in sinoatrial node (SAN), AC1 and AC8, are activated by $Ca^{2+}$/calmodulin and insensitive to subunit of heterotrimeric G proteins (Gαs) in vitro[5,6]. In pacemaker cells,

71 the AC8-cAMP-PKA signaling pathway induces the phosphorylation of $Ca^{2+}$ cycling
72 proteins to generate the action potential[5]. In our previous work using the mouse model
73 with cardiac specific overexpression of human AC8 gene (TGAC8), we have discovered
74 that the heart rate (HR) of TGAC8 is increased approximately 30% compared with the
75 wild-type (WT) littermate, and the intrinsic coupled-clock system (in the absence of β1-
76 ARs stimulation) within the SAN cells is crucially dependent on the activation of AC8,
77 but the overall pattern of marked coherency or loss of complexity (HR variability) within
78 the TGAC8 heart rhythm is similar to that associated with aging or cardiac pathology[7].
79 Although we have already profiled the changes in the TGAC8 mouse left ventricle (LV)
80 at RNA, protein and phosphorylation levels[8,9], and have characterized the various cellular
81 functions at single nucleus resolution in C57/BL6 mouse SAN[10], the molecular
82 mechanisms, especially the transcriptomic regulation in SAN, by which TGAC8
83 regulates SAN functions and its long-term effect, remain elusive.

84 To unravel the underlying molecular mechanisms, in the present research, we conducted
85 deep RNA sequencing (RNA-seq) to profile the SAN transcriptome in mouse (TGAC8
86 vs. WT). Utilizing multiple bioinformatic techniques, we enriched representative
87 pathways and discovered an unexpected downregulation of components and functions of
88 mitochondria and ribosome, which may be associated with CVDs in long term of chronic
89 activation of AC8 in the heart. Our results provide valuable transcriptomic data for
90 further research on the regulation in cardiac function, especially through the ACs-cAMP-
91 PKA signaling pathway.

92

93 # Materials and Methods

94 ## 1. Animals.

95 The cardiac-specific overexpression of AC8 (TGAC8) mouse, generated by inserting a
96 cDNA coding for human AC8 after the murine a-myosin heavy chain promoter[6], was a
97 gift from Nicole Defer/Jacques Hanoune, Unite de Recherches, INSERM U-99, Hôpital
98 Henri Mondor, F-94010 Créteil, France. Twelve-week old male TGAC mice were used as
99 study cases, and age matched WT littermates, in the C57/BL6 background, were used as
100 controls. All studies were performed in accordance with the Guide for the Care and Use
101 of Laboratory Animals published by the National Institutes of Health (NIH Publication
102 no. 85-23, revised 1996). The experimental protocols were approved by the Animal Care
103 and Use Committee of the National Institutes of Health (protocol #441-LCS-2016).

104

105 ## 2. Sinoatrial node (SAN) and SAN cell isolation.

106 SAN and SAN cells were isolated in the same way described in our previous paper[7].
107 Briefly, after anesthetization of TGAC8 and WT mice, the hearts were quickly removed
108 and SANs were dissected between inferior and superior vena cava, crista terminalis, and
109 intra-atrial septum and cut into strips perpendicular to the crista terminalis. The isolated
110 SANs were washed (X3) in the modified low $Ca^{2+}$ Tyrode solution before enzymatic
111 digestion. The digested SANs were washed (X3) in modified high potassium solution
112 before dispersion by gentle pipetting. The dispersed SAN cells were stored at 4°C for
113 following experiments.

114

## 3. RNA extraction, cDNA library preparation, and RNA-seq.

By company. We sent eight TGAC8 and eight WT mouse SANs to DNA Link USA company to conduct total RNA-seq. RNAs were extracted from each SNAs separately and used as template for cDNA library preparation following the instruction manual of SMARTer Stranded Total RNA-Seq Kit-Pico/Clontech Laboratories, Lnc. The sequencing was conducted on the Illumina NextSeq 500 platform and the data were obtained within the basecaling software RTA2.0.

## 4. RNA-seq data processing.

The raw reads were trimmed within Cutadapt and aligned within SAMtools. Using Mm10plus and ADCY8 as the reference genome, the aligned reads were mapped to calculate the raw counts. After quality control and filtration, we selected six WT samples (WS1, WS2, WS3, WS4, WS5 and WS 8) and five TGAC8 samples (MS1, MS2, MS4, MS5 and MS8) for the subsequent differential expression gene (DEG) analysis using DESeq2 package in R language, and identified 16575 genes. The normalized counts by DESeq2 were imported into Partek Flow to perform PCA and generate expression heat map. Furtherly, we calculated sample distances using the Euclidean method for rows and columns distance clustering and generated matrix using the ward.D method for matrix clustering in R language. The adjusted p-value and fold change calculated by DESeq2 were used to draw volcano plot to figure out the expression changes of TGAC8 SAN transcriptome. Specifically, 352 genes were downregulated (-log10(adjusted p-value) > 1.3 and log2(fold change) < 0) and 323 upregulated ((-log10(adjusted p-value) > 1.3 and log2(fold change) > 0).

138

139 ## 5. Marker genes selection and analysis.

140 The expressions of several families of genes encoding proteins related to ion channels
141 and AC8-cAMP-PKA pathway, i.e., sodium/calcium exchanger in solute carrier family
142 (Slc), hyperpolarization activated cyclic nucleotide gated potassium channel (Hcn), S100
143 calcium binding protein (S100), sodium voltage-gated channel (Na+), potassium voltage-
144 gated channel (K+), calcium voltage-gated channel (Ca2+), stromal interaction molecule
145 (Stim), phosphodiesterase (Pde), protein kinase CAMP-dependent regulation proteins
146 (PKA), and sarcolipin (Sln), were extracted from TGAC8 SAN RNA-seq data and
147 visualized in heat map. The significant changes of these genes were further displayed in
148 volcano plot and bar plot. All analyses were performed and all plots were produced in R
149 language.

150

151 ## 6. Ingenuity pathway analysis (IPA).

152 All identified genes were uploaded to IPA software (QIAGEN, March 2020)[11]. The
153 Ingenuity knowledge base (gene only) about all species and all tissues was selected as the
154 reference set. All Ingenuity supported third party information and Ingenuity expert
155 information were adopted as the data sources, and only experimentally observed
156 relationships were selected to increase confidence. Setting the cutoff as adjusted p-value
157 $< 0.05$, IPA recognized 636 differential expressed genes, including 321 down and 315 up,
158 which were used for subsequent canonical pathway analysis, upstream regulator
159 prediction, disease state analysis match, and regulatory pathway construction.
160 Specifically, OXPHOS pathway and apelin cardiomyocyte signaling pathway were

161 visualized, and the regulatory pathway starting from KDM5A and PPARGC1A was
162 generated in IPA.
163

## 164 7. KEGG pathway analysis using pathfindR package.

165 To reduce the redundancy and find the most important pathways, KEGG pathway
166 analysis was performed using pathfindR package in R language[12]. The KEGG mouse
167 (mmu) database was used as background gene set. Besides normal KEGG enrichment, we
168 generated term-gene graph to cluster all pathways into seven clusters and select the hub
169 pathway in each cluster. We also displayed the pathway level heat map for individual
170 sample to clarify the contribution of each sample to the pathway enrichment.
171

## 172 8. Gene set enrichment analysis (GSEA).

173 To take all identified genes into consideration and preclude bias due to arbitrary cutoff,
174 we uploaded all identified genes into GSEA software[13] for analyses within four
175 databases, KEGG, GO_BP, GO_CC, and GO_MF. The software can recognize 16571
176 native features. After collapsing features into gene symbols, there are 12873 genes
177 remained. The calculation parameters in GSEA were as below: (1) gene-set permutation;
178 (2) permutation number: 1000; (3) scoring_scheme: weighted; (4) norm: meandiv; (5)
179 mode: Max_probe; (6) include_only_symbols: true; (7) set_max: 500; (8) set_min: 15;
180 (9) metric: Signal2Noise; (10) order: descending. The top 20 significantly enriched
181 pathways sorted by normalized enrichment score (NES) within each database were used
182 for generation of bubble graphs and representative GSEA enrichment plots.
183

## 9. RNA extraction, cDNA synthesis, qRT-PCR, and data analysis.

The preparation for and performance of qRT-PCR were done as stated in our previous paper in detail[7]. Briefly, RNAs were extracted from isolated mouse SAN with RNeasy Mini Kit (Qiagen, Valencia, CA, United States) and DNAse. 2 mg of total RNA was used for cDNA synthesis with MMLV reverse transcriptase (Promega) in final 50 mL volume. Primers used for each transcript assessed are listed in Supplementary Table (in preparation). qRT-PCR was performed on QuantStudio 6 Flex Real-Time PCR System (Thermo Fisher Scientific) with 384-well platform. Reaction was performed with FastStart Universal SYBR Green Master Kit with Rox (Roche). Normalized to expression of HPRT level, qRT-PCR analysis was performed using ddCt method.

## 10. Statistical analyses.

Transcriptomic data were processed in Partek® Flow® software, version 9.0 Copyright ©; 2020 Partek Inc., St. Louis, MO, USA, by utilizing the computational resources of the NIH HPC Biowulf cluster (http://hpc.nih.gov). Most statistical analyses were performed using RStudio (version: 1.1.463) in R language (version: 3.5.3). Some other data processing and statistics were conducted in GraphPad Prism (version: 7) and Microsoft Excel (version: 2019). Adobe Illustrator (version: CC 2019) were also used for graphics without changing data trend or structure. For qRT-PCR analysis, the two-sided unpaired Student's t-test was used to compare the mRNA expression between TGAC8 and WT SAN, and p-value $< 0.05$ was taken as statistically significant.

# Results

## 1. RNA sequencing on mouse SAN tissue.

To study the molecular mechanism, we isolated SANs from twelve-week-old male TGAC8 mice and their WT littermates to conduct deep RNA sequencing (RNA-seq). TG and WT samples were separated into two groups in primary components analysis (PCA) (Figure A1). Furtherly, we calculated sample distances and observed that the inner group sample distance was smaller than inter group sample distance (Figure 1B). We also scaled and visualized the expressions of all identified genes in heatmap, and observed two hierarchical clusters, indicating the differential regulation between the two groups of samples (Figure 1C). Setting the cutoff as -log10(adjusted p-value) > 1.3, i.e., adjusted p-value < 0.05, we obtained 675 differentially regulated (up and down) genes, among which 352 genes were downregulated (down) and 323 upregulated (up) (Figure 1D).

As SAN is the main pacemaker of the heart and AC8-cAMP-PKA axis is pivotal to excitation-contraction coupling, we profiled the expression of several families of genes encoding proteins related to ion channels and AC8-cAMP-PKA pathway, i.e., sodium/calcium exchanger in solute carrier family (Slc), hyperpolarization activated cyclic nucleotide gated potassium channel (Hcn), S100 calcium binding protein (S100), sodium voltage-gated channel ($Na^+$), potassium voltage-gated channel ($K^+$), calcium voltage-gated channel ($Ca^{2+}$), stromal interaction molecule (Stim), phosphodiesterase (Pde), protein kinase cAMP-dependent regulation proteins (PKA), and sarcolipin (Sln) (Figure 2A), among which there were 13 genes regulated significantly by overexpression of AC8 (Figure 2B). Particularly, one member in solute carrier family, Slc8a3, was increased most significantly (Figure 1D and Figure 2C), and two members in phosphodiesterase were also upregulated as feedback to the overexpression of AC8 to

230 finetune the content of cAMP inside SAN (Figure 2C). The characterization of RNA-seq
231 data demonstrated that the cardiac-specific overexpression of AC8 reprogramed the
232 transcriptome in SAN and regulated expression of genes related to cardiac functions.

233

## 234 2. Functional enrichment of TGAC8 SAN transcriptome.

235 To reveal the functions of the reprogramed SAN transcriptome, we performed functional
236 analysis using Ingenuity Pathway Analysis (IPA) software. The top 25 enriched canonical
237 pathways sharing same genes interacted with each other. As expected, protein kinase A
238 signaling was in the center of the aggregated pathways (Figure 3A), confirming the
239 activation of AC8-cAMP-PKA signaling pathway in our transgenic mouse model
240 (TGAC8). With enrichment p-value and activation prediction z-score, pathways related to
241 mitochondrial functions were unexpectedly enriched and ranked at the top, sorted by -
242 log10(p-value) (Figure 3B).

243 We also conducted KEGG pathway analysis using pathfindR package in R language to
244 study the functions of TGAC8 SAN transcriptome from another respect. Similar to
245 results from IPA, oxidative phosphorylation (OXPHOS) pathway was also enriched and
246 ranked as the top pathway among all enriched KEGG pathways (Figure 4A). Many genes
247 were shared by multiple pathways (Figure 4B-4C), so to reduce the redundancy and find
248 the most important molecular pathways, we clustered the enriched pathways into seven
249 clusters, from which we selected one hub pathway as the representative for each pathway
250 cluster (Figure 4D). The OXPHOS pathway was still the most significant pathway as the
251 hub in cluster 1. In addition, ribosome and cardiac muscle contraction were also enriched
252 and served as the hub in cluster 2 and cluster 3 respectively (Figure 4D). Interestingly,

253 from the term-gene graph and pathway heatmap, we observed that the majority of
254 associated genes were downregulated, especially genes in the top three hub pathways,
255 i.e., OXPHOS, ribosome, and cardiac muscle contraction (Figure 4B-4C, 4E). Therefore,
256 the regulation of these three pathways may be the molecular mechanism underlying the
257 TGAC8 SAN transcriptome, and we continued to analyze them in depth.

258

259 **3. Suppressed mitochondria and mitochondrial function pathways.**

260 The fitness of SAN relies on normal mitochondrial functions to generate enough energy
261 and maintain energy homeostasis. The above analyses in IPA and KEGG, with the cutoff
262 p-value < 0.05, had already implied the inhibition of mitochondrial function in TGAC8
263 mouse. To take all identified genes into consideration, we made use of gene set
264 enrichment analysis (GSEA). In congruent with the above analyses, many mitochondrial
265 components and mitochondrial functions were enriched without the requirement of any
266 cutoff of p-value or fold change in GSEA (Figure 5A). Regardless of the cutoff, more
267 genes in the gene set of OXPHOS were used for calculation and most genes were still
268 enriched as downregulated in TGAC8 mouse, as shown in the representative GSEA
269 enrichment plots (Figure 5B). Therefore, multiple functional enrichment methods,
270 including IPA, pathfindR, and GSEA, drew the same conclusion: suppressed
271 mitochondria and mitochondrial function in TGAC8 vs. WT.

272 To visualize individual differentially regulated gene related to mitochondria and
273 mitochondrial function, we visualized the OXPHOS pathway within IPA. Significantly
274 regulated genes (adjusted p-value < 0.05) encode subunits in OXPHOS complex I, III, IV

275 and V (colored with purple outlines), and all of them were downregulated (filled in green)
276 (Figure 5C).

277 To confirm the RNA-seq results, we would perform q-RT PCR to evaluate the expression
278 of the transcribed mRNAs. Mitochondrial function was also analyzed via WB, activity
279 kits, and seahorse analysis, especially for complex I, III, IV, and V.

280

281 **4. Suppressed ribosome and translation pathways.**

282 The translation process is one stage of the cell protein quality control, which consumes
283 large amount of energy produced in mitochondria. Mitochondria, as a semi-autonomic
284 organelle, consists of proteins that are synthesized in cytoplasm and mitochondria itself.
285 The majority of mitochondrial proteins are translated by cytosolic ribosome, and a small
286 portion is translated by mitochondrial ribosome. The enrichment of ribosome as the hub
287 in cluster 2 of KEGG pathways (Figure 4D) prompted us to further analyze ribosome and
288 translation. In agreement with the enrichments of both cytosolic ribosome and
289 mitochondrial ribosome subunits, translation inside and outside of mitochondria were
290 also enriched in GSEA (Figure 6A). In line with the downregulation of genes related to
291 ribosome that were displayed in term-gene graph (Figure 3B), the peaks in GSEA
292 enrichment plots of ribosome and translation were downward, indicating the suppression
293 of translation (Figure 6B). Particularly, the inhibited mitochondrial ribosome and
294 mitochondrial translation implied the possible reciprocal regulation between
295 mitochondria and ribosome: suppressed mitochondria produce less energy for translation,
296 while downregulated ribosome and weakened translation generate fewer mitochondrial
297 proteins.

298 We would perform qRT-PCR to confirm the downregulated transcription of ribosomal
299 components and do protein synthesis detection and WB to verify the suppressed
300 translation.

301

302 **5. Association with impaired cardiac functions.**

303 Intriguingly, only inositol phosphate related pathways were significantly positively
304 enriched within GSEA (Figure 7). As a family of calcium channels, inositol 1,4,5-
305 trisphosphate receptors (IP3Rs) are ubiquitously expressed in all tissues[8]. In the heart,
306 IP3Rs have been associated with regulation of cardiomyocyte function ranging from the
307 regulation of pacemaking, excitation–contraction and excitation–transcription
308 coupling[14,15]. The upregulated inositol phosphate increases the inner cellular $Ca^{2+}$ to
309 enhance cardiac contraction[14,15], which perhaps mediates the effect of overexpression of
310 AC8 to increase the HR[7]. However, the abnormally activated IP3Rs signaling may
311 contribute to CVDs, like arrhythmias, hypertrophy and heart failure[14,15]. Mechanistically,
312 inositol 1,4,5-trisphosphate (IP3) is involved in the flow of $Ca^{2+}$ between mitochondria
313 and endoplasmic/sarcoplasmic reticulum[16]. In cardiomyocytes, IP3 regulates
314 mitochondrial $Ca^{2+}$ uptake through the mitochondrial ryanodine receptor (RyR) to
315 influence adenosine triphosphate (ATP) production, which may be one mechanism how
316 abnormal inositol phosphate metabolism impairs the cardiac function[17].

317 In terms of cardiac function, we enriched apelin cardiomyocyte signaling pathway in IPA
318 (Figure 3B). Apelin plays an important role in the regulation of cardiac functions,
319 including inducing vasodilation, raising contractility and HR, and reducing reperfusion
320 injury[18-20]. From the apelin cardiomyocyte signaling pathway generated in IPA, we

321 observed that the transcriptional expression of myosin light chain genes was decreased in
322 TGAC8 vs. WT, but the transcriptional expression of genes encoding several enzymes,
323 including phosphatidylinositol-4,5-bisphosphate 3-kinase, phospholipase C, and protein
324 kinase C, was increased in TGAC8 vs. WT (Figure 8A). To corroborate the enrichment of
325 KEGG pathway, cardiac muscle contraction (Figure 4), we searched the enriched
326 pathways within GSEA and found expression of most genes in the cardiac muscle
327 contraction pathway was declined and the peak was downward in TGAC8 mouse (Figure
328 8B). The two enrichments in IPA and KEGG prompted us to further study the possibility
329 of cardiac function impairment.

330 By the utilization of databases in IPA, we compared the TGAC8 mouse SAN
331 transcriptome with all available public projects and displayed the analysis match in
332 Figure 7C. Obviously, there were more matched disease projects with positive z-score,
333 indicating that TGAC8 SAN transcriptome was more comparable to/like heart disease
334 states than normal state (Figure 8C). Therefore, the reprogramed SAN transcriptome
335 implied that the chronic overexpression of AC8 in the heart increases the HR at the cost
336 of cardiac function and may result in/be associated with CVDs in long term.

337

## 338 6. Regulatory pathway of TGAC8 SAN transcriptome.

339 To clarify the mechanistic pathway, we performed the prediction of possible upstream
340 regulators mediating the effect of overexpression of AC8 to reprogram the SAN
341 transcriptome. As RNA-seq data mainly reflects the regulation at transcriptional level, we
342 first set the filter to screen all transcription regulators. Many predicted upstream
343 regulators were also identified as significantly changed genes in the TGAC8 SAN

344 transcriptome, so we set the second filter to select those genes whose transcriptional
345 expression was changed in the same direction to the trend of predicted activation. Finally,
346 we ranked all remained genes by B-H corrected p-value of prediction. Two regulators,
347 PPARGC1A and KDM5A, were the most significantly inhibited and activated factors
348 respectively. Peroxisome proliferator-activated receptor gamma coactivator 1-alpha
349 (PGC-1α), encoded by the *PPARGC1A* gene[21], interacts with many other regulators,
350 including peroxisome proliferator-activated receptor gamma (PPAR-γ or PPARG), cAMP
351 response element-binding protein (CREB), and nuclear respiratory factors (NRFs)[22-24], to
352 regulate mitochondrial biogenesis and energy metabolism[25]. Lysine-specific demethylase
353 5A (KDM5A) is encoded by the *KDM5A* gene[26], and its loss restores mitochondrial
354 function in cells lacking Rb1, partly by activating PGC-1α[27]. Therefore, we presumed the
355 two transcription regulators as the mediators of the effect of overexpression of AC8 in
356 SAN, and thus we established a regulatory pathway starting from the two regulators
357 within IPA (Figure 9A). In the established pathway, the majority of genes under the
358 control of the two regulators encode subunits in mitochondrial complex I, III, IV and V,
359 whose downregulations contribute to mitochondrial dysfunction and disrupted OXPHOS
360 process. In addition, the protein, Mitochondrial Ribosome Protein L53 (MRPL53), which
361 is translated from one downstream gene whose expression is under the control of
362 KDM5A, is a subunit of mitochondrial ribosome, and another protein, Translocase Of
363 Outer Mitochondrial Membrane 7 (TOMM7), which is translated from another gene, is
364 important in import of molecules into mitochondria. Therefore, the activated KDM5A
365 could also suppress other mitochondrial functions such as mitochondrial translation and
366 transport.

367

368 ## Discussion

369 In SAN, the ACs-cAMP-PKA signaling pathway plays an important role in
370 pacemaking[3,5]. Previously, we discovered that the cardiac-specific overexpression of AC8
371 elevates the HR, but the overall pattern of marked coherency or loss of complexity (HR
372 variability) within the TGAC8 heart rhythm is similar to that associated with aging or
373 cardiac pathology[7]. In this research, we conducted RNA-seq to analyze the SAN
374 transcriptome to reveal the underlying molecular mechanism and envisioned a possible
375 long-term effect of chronic overexpression of AC8 in the heart. As expected, we observed
376 obvious reprogramming in the SAN transcriptome (Figure 1-2). Beyond our expectation,
377 it was mitochondrial function that was enriched most significantly and consistently in all
378 analyses using multiple bioinformatic methods. We also enriched the suppressed
379 ribosome and translation, and promoted inositol metabolism. Integrating all analyses, we
380 deduced a schematic (Figure 9B). The cardiac-specific overexpression of AC8 suppresses
381 ribosome and translation, and mitochondria and their functions, while promotes inositol
382 phosphate and its metabolism. Two transcription regulators, KDM5A and PPARGC1A,
383 may mediate the effect of overexpression of AC8 on ribosome and mitochondria. The
384 abnormal ribosome and inositol phosphate could also cross talk with mitochondria to
385 disrupt mitochondrial functions. In long term, the chronic overexpression of AC8
386 increases HR overtime at the cost of impaired SAN functions, perhaps resulting
387 in/associated with CVDs.

388

389 **1. Why does TGAC8 mouse SAN inhibit mitochondria and ribosome while**
390 **activating inositol phosphate metabolism?**

391 In our previous work, we observed the elevated HR in TGAC8 mouse relative to WT
392 mouse[7]. The high-intensive and restless cardiac contraction lays a heavy load on energy
393 production in mitochondria, which is the hub of energy homeostasis and metabolic
394 homeostasis. The energy in shortage is hard to meet the demand for protein synthesis and
395 cardiac contraction at the same time, so the translation could be sacrificed, as shown in
396 the enrichments of suppressed ribosome components and translation in this research. The
397 temporary or moderate decline of translation could induce several beneficial stress
398 responses, including endoplasmic reticulum (ER) unfolded protein response (UPR)
399 ($UPR^{er}$) and mitochondrial UPR ($UPR^{mt}$), to improve the protein quality control[28].
400 Interrogating the processed TGAC8 SAN RNA-seq data, we found some factors involved
401 in UPR were upregulated, e.g., Atf6, Mbtps1, Mbtps2, Ern1, etc.

402 On the other hand, the regulated mitochondrial function is often accompanied with
403 altered metabolism. Inositol phosphate, a type of metabolic derivative from lipids, is
404 often localized in plasma membrane[29], where it affects $Ca^{2+}$ release from intracellular
405 stores[30] and regulates $Ca^{2+}$ flow between mitochondria and endoplasmic/sarcoplasmic
406 reticulum[16]. In the heart, the upregulated inositol phosphate increases the inner cellular
407 $Ca^{2+}$ to enhance cardiac contraction[14,15], which may be an additional arm to PKA pathway
408 in mediating the effect of activation of AC8 to increase the HR[7]. Therefore, TGAC8
409 mouse SAN prefers to inhibit mitochondria and ribosome while activate inositol
410 phosphate metabolism to maintain high-intensive cardiac contraction.

411

412 ## 2. How do the regulated pathways mediate the effect of TGAC8 in long term?

413 The three hub pathways, mitochondrial function (Figure 5), ribosome and translation
414 (Figure 6), and inositol metabolism (Figure 7), were not distinct from each other.
415 Mitochondria not only produce energy for protein synthesis, but also control metabolism
416 to impact inositol phosphate indirectly. In turn, the assembly of complete functional
417 mitochondrial complex relies on proteins synthesized in cytosol and mitochondria. IP3
418 regulates mitochondrial $Ca^{2+}$ uptake to influence ATP production[17]. Although the
419 temporary or moderate protein stress and mitochondrial stress are beneficial to health, the
420 long-term and vigorous stress is detrimental to health[31]. For example, the elevated HR
421 increases blood supply in response to exercise or emergency, but it aggravates the burden
422 of heart in the context of chronic heart diseases. Similarly, the abnormally and
423 persistently activated IP3Rs signaling may result in arrhythmias, hypertrophy and even
424 heart failure[14,15]. Under chronic CVDs states, UPR may be maladaptive[32], exemplified by
425 its arrhythmic effect during human heart failure by affecting cardiac ion channels
426 expression[33]. The persistent UPR could also be an upstream signal to promote cancer[34].
427 In our TGAC8 mouse model, we observed elevated HR as a chronic stress laid on mouse
428 heart[7]. The enriched cardiac function pathways, especially downregulated cardiac
429 contraction pathway, predict a coming cardiac disorder, in line with a recently published
430 work where aggravated age-related myocardial dysfunction was reported in TGAC8 mice
431 compared with their WT littermates[35]. Therefore, our results not only support the concept
432 of detrimental role of chronic stress, but also indicate the association of early-stage
433 reprogramming of SAN transcriptome with the late-stage cardiac pathology.

434

## 3. Can we regulate these pathways to ameliorate the side-effect of TGAC8 in long term?

As the robust functions of ribosome and mitochondria are pivotal to health, the ideal way to improve cardiac fitness is to concurrently enhance cardiac contraction and biological processes, i.e., OXPHOS, translation, and metabolism, to maintain cardiac homeostasis at a higher level. The TGAC8 has already elevated the HR, so we need to increase the functions of ribosome and mitochondria to maintain health. Two transcription regulators, KDM5A and PPARGC1A (PGC-1α), were predicted to be the mediators in TGAC8 to inhibit ribosome and mitochondria. The expression of KDM5A was reported to be negatively correlated with subunits in mitochondrial complexes[27], and PGC-1α is well known as a positive regulator of mitochondrial biogenesis[25]. Therefore, the two regulators have the potential to be therapeutic targets in improving SAN functions, particularly in aged TGAC8 mouse, or patients under similar chronic stresses.

## 4. Limitation.

We unraveled the reprogramed transcriptome in TGAC8 vs. WT SAN, which indicates the suppressed components and function of ribosome and mitochondria, along with promoted inositol phosphate metabolism, but more wet lab experiments were not included in this research due to the scarcity of isolated SAN samples. In addition, the complete and clear signaling pathway, from AC8 to mediators, to target genes, and to downstream effects, need further validation. For example, the double gene mutation mouse models, e.g., $TG^{AC8}$-$TG^{PPARGC1A}$ or $TG^{AC8}$-$KO^{KDM5A}$ mouse, could be used to in-depth study the regulatory mechanisms of overexpression of AC8 in SAN and to reveal potential therapeutic targets of chronic CVDs, especially during aging.

## Acknowledgements

We thank all members in Laboratory of Cardiovascular Science, National Institute on Aging, National Institutes of Health, for technical assistance and discussion. This work utilized the computational resources of the NIH HPC Biowulf cluster (http://hpc.nih.gov).

## Funding

Intramural Research Program, National Institute on Aging, National Institutes of Health.

## Disclosures

None.

## Reference

1 **Chiao, Y. A. & Rabinovitch, P. S. The Aging Heart. *Cold Spring Harb Perspect Med* 5, a025148 (2015). https://doi.org:10.1101/cshperspect.a025148**

2 **Strait, J. B. & Lakatta, E. G. Aging-associated cardiovascular changes and their relationship to heart failure. *Heart Fail Clin* 8, 143-164 (2012). https://doi.org:10.1016/j.hfc.2011.08.011**

3 **Guellich, A., Mehel, H. & Fischmeister, R. Cyclic AMP synthesis and hydrolysis in the normal and failing heart. *Pflugers Arch* 466, 1163-1175 (2014). https://doi.org:10.1007/s00424-014-1515-1**

4 **de Lucia, C., Eguchi, A. & Koch, W. J. New Insights in Cardiac beta-Adrenergic Signaling During Heart Failure and Aging. *Front Pharmacol* 9, 904 (2018). https://doi.org:10.3389/fphar.2018.00904**

5 **Vinogradova, T. M. & Lakatta, E. G. Regulation of basal and reserve cardiac pacemaker function by interactions of cAMP-mediated PKA-dependent Ca2+ cycling with surface membrane channels. *Journal of molecular and cellular cardiology* 47, 456-474 (2009). https://doi.org:10.1016/j.yjmcc.2009.06.014**

488 6 Lipskaia, L. *et al.* Enhanced cardiac function in transgenic mice expressing a
489 Ca(2+)-stimulated adenylyl cyclase. *Circ. Res.* 86, 795-801 (2000).
490 https://doi.org:10.1161/01.res.86.7.795
491 7 Moen, J. M. *et al.* Overexpression of a Neuronal Type Adenylyl Cyclase (Type
492 8) in Sinoatrial Node Markedly Impacts Heart Rate and Rhythm. *Front*
493 *Neurosci* 13, 615 (2019). https://doi.org:10.3389/fnins.2019.00615
494 8 Tarasov, K. V. *et al.* A remarkable adaptive paradigm of heart performance
495 and protection emerges in response to the constitutive challenge of marked
496 cardiac-specific overexpression of adenylyl cyclase type 8. *eLife* 11, e80949
497 (2022). https://doi.org:10.7554/eLife.80949
498 9 Qu, J.-H. *et al.* Reprogramming of the cardiac phosphoproteome in
499 conjunction with proteome and transcriptome creates the enhanced
500 performance and protection circuitry in response to chronic adenylyl cyclase-
501 driven stress. *bioRxiv*, 2022.2004.2029.488779 (2023).
502 https://doi.org:10.1101/2022.04.29.488779
503 10 Qu, J. H., Telljohann, R., Byshkov, R. & Lakatta, E. G. Characterization of
504 diverse populations of sinoatrial node cells and their proliferation potential
505 at single nucleus resolution. *Heliyon* 9, e12708 (2023).
506 https://doi.org:10.1016/j.heliyon.2022.e12708
507 11 Kramer, A., Green, J., Pollard, J., Jr. & Tugendreich, S. Causal analysis
508 approaches in Ingenuity Pathway Analysis. *Bioinformatics (Oxford, England)*
509 30, 523-530 (2014). https://doi.org:10.1093/bioinformatics/btt703
510 12 Ulgen, E., Ozisik, O. & Sezerman, O. U. pathfindR: An R Package for
511 Comprehensive Identification of Enriched Pathways in Omics Data Through
512 Active Subnetworks. *Front Genet* 10, 858 (2019).
513 https://doi.org:10.3389/fgene.2019.00858
514 13 Subramanian, A. *et al.* Gene set enrichment analysis: A knowledge-based
515 approach for interpreting genome-wide expression profiles. *Proceedings of*
516 *the National Academy of Sciences* 102, 15545-15550 (2005).
517 https://doi.org:10.1073/pnas.0506580102
518 14 Garcia, M. I. & Boehning, D. Cardiac inositol 1,4,5-trisphosphate receptors.
519 *Biochim Biophys Acta Mol Cell Res* 1864, 907-914 (2017).
520 https://doi.org:10.1016/j.bbamcr.2016.11.017
521 15 Kockskamper, J. *et al.* Emerging roles of inositol 1,4,5-trisphosphate
522 signaling in cardiac myocytes. *Journal of molecular and cellular cardiology*
523 45, 128-147 (2008). https://doi.org:10.1016/j.yjmcc.2008.05.014
524 16 Jaconi, M. *et al.* Inositol 1,4,5-trisphosphate directs Ca2+ flow between
525 mitochondria and the endoplasmic/sarcoplasmic reticulum: A role in
526 regulating cardiac autonomic Ca2+ spiking. *Mol. Biol. Cell* 11, 1845-1858
527 (2000). https://doi.org:10.1091/mbc.11.5.1845
528 17 Seidlmayer, L. K. *et al.* Inositol 1,4,5-trisphosphate-mediated sarcoplasmic
529 reticulum-mitochondrial crosstalk influences adenosine triphosphate
530 production via mitochondrial Ca2+ uptake through the mitochondrial
531 ryanodine receptor in cardiac myocytes. *Cardiovascular research* 112, 491-
532 501 (2016). https://doi.org:10.1093/cvr/cvw185

533 18 Berry, M. F. *et al.* Apelin has in vivo inotropic effects on normal and failing
534 hearts. *Circulation* 110, Ii187-193 (2004).
535 https://doi.org:10.1161/01.CIR.0000138382.57325.5c
536 19 Ashley, E. A. *et al.* The endogenous peptide apelin potently improves cardiac
537 contractility and reduces cardiac loading in vivo. *Cardiovascular research* 65,
538 73-82 (2005). https://doi.org:10.1016/j.cardiores.2004.08.018
539 20 Szokodi, I. *et al.* Apelin, the novel endogenous ligand of the orphan receptor
540 APJ, regulates cardiac contractility. *Circ. Res.* 91, 434-440 (2002).
541 https://doi.org:10.1161/01.res.0000033522.37861.69
542 21 Esterbauer, H., Oberkofler, H., Krempler, F. & Patsch, W. Human
543 peroxisome proliferator activated receptor gamma coactivator 1 (PPARGC1)
544 gene: cDNA sequence, genomic organization, chromosomal localization, and
545 tissue expression. *Genomics* 62, 98-102 (1999).
546 https://doi.org:10.1006/geno.1999.5977
547 22 Wallberg, A. E., Yamamura, S., Malik, S., Spiegelman, B. M. & Roeder, R. G.
548 Coordination of p300-mediated chromatin remodeling and TRAP/mediator
549 function through coactivator PGC-1alpha. *Molecular cell* 12, 1137-1149
550 (2003). https://doi.org:10.1016/s1097-2765(03)00391-5
551 23 Puigserver, P. *et al.* Activation of PPARgamma coactivator-1 through
552 transcription factor docking. *Science* 286, 1368-1371 (1999).
553 https://doi.org:10.1126/science.286.5443.1368
554 24 Wu, Z. *et al.* Mechanisms controlling mitochondrial biogenesis and
555 respiration through the thermogenic coactivator PGC-1. *Cell* 98, 115-124
556 (1999). https://doi.org:10.1016/s0092-8674(00)80611-x
557 25 Dorn, G. W., 2nd, Vega, R. B. & Kelly, D. P. Mitochondrial biogenesis and
558 dynamics in the developing and diseased heart. *Genes & development* 29,
559 1981-1991 (2015). https://doi.org:10.1101/gad.269894.115
560 26 Defeo-Jones, D. *et al.* Cloning of cDNAs for cellular proteins that bind to the
561 retinoblastoma gene product. *Nature* 352, 251-254 (1991).
562 https://doi.org:10.1038/352251a0
563 27 Váraljai, R. *et al.* Increased mitochondrial function downstream from
564 KDM5A histone demethylase rescues differentiation in pRB-deficient cells.
565 *Genes & development* 29, 1817-1834 (2015).
566 https://doi.org:10.1101/gad.264036.115
567 28 Zhang, R. *et al.* Caloric Restriction Induces MicroRNAs to Improve
568 Mitochondrial Proteostasis. *iScience* 17, 155-166 (2019).
569 https://doi.org:https://doi.org/10.1016/j.isci.2019.06.028
570 29 Lyall, F. in *Basic Science in Obstetrics and Gynaecology (Fourth Edition)* (eds
571 Phillip Bennett & Catherine Williamson) 143-171 (Churchill Livingstone,
572 2010).
573 30 Hughes, A. R. & Putney, J. W., Jr. Inositol phosphate formation and its
574 relationship to calcium signaling. *Environmental health perspectives* 84, 141-
575 147 (1990). https://doi.org:10.1289/ehp.9084141
576 31 Li, X. *et al.* Targeting mitochondrial reactive oxygen species as novel therapy
577 for inflammatory diseases and cancers. *J. Hematol. Oncol.* 6, 19-19 (2013).
578 https://doi.org:10.1186/1756-8722-6-19

579 32 Arrieta, A., Blackwood, E. A. & Glembotski, C. C. ER Protein Quality
580 Control and the Unfolded Protein Response in the Heart. *Current topics in*
581 *microbiology and immunology* 414, 193-213 (2018).
582 https://doi.org:10.1007/82_2017_54
583 33 Liu, M. & Dudley, S. C., Jr. Role for the Unfolded Protein Response in Heart
584 Disease and Cardiac Arrhythmias. *Int. J. Mol. Sci.* 17, 52 (2015).
585 https://doi.org:10.3390/ijms17010052
586 34 Santamaría, P. G., Mazón, M. J., Eraso, P. & Portillo, F. UPR: An Upstream
587 Signal to EMT Induction in Cancer. *J Clin Med* 8, 624 (2019).
588 https://doi.org:10.3390/jcm8050624
589 35 Mougenot, N. *et al.* Cardiac adenylyl cyclase overexpression precipitates and
590 aggravates age-related myocardial dysfunction. *Cardiovascular research* 115,
591 1778-1790 (2019). https://doi.org:10.1093/cvr/cvy306

592

593

594

595

596

597

598

599

600

601

602

603

# Figures and Legends

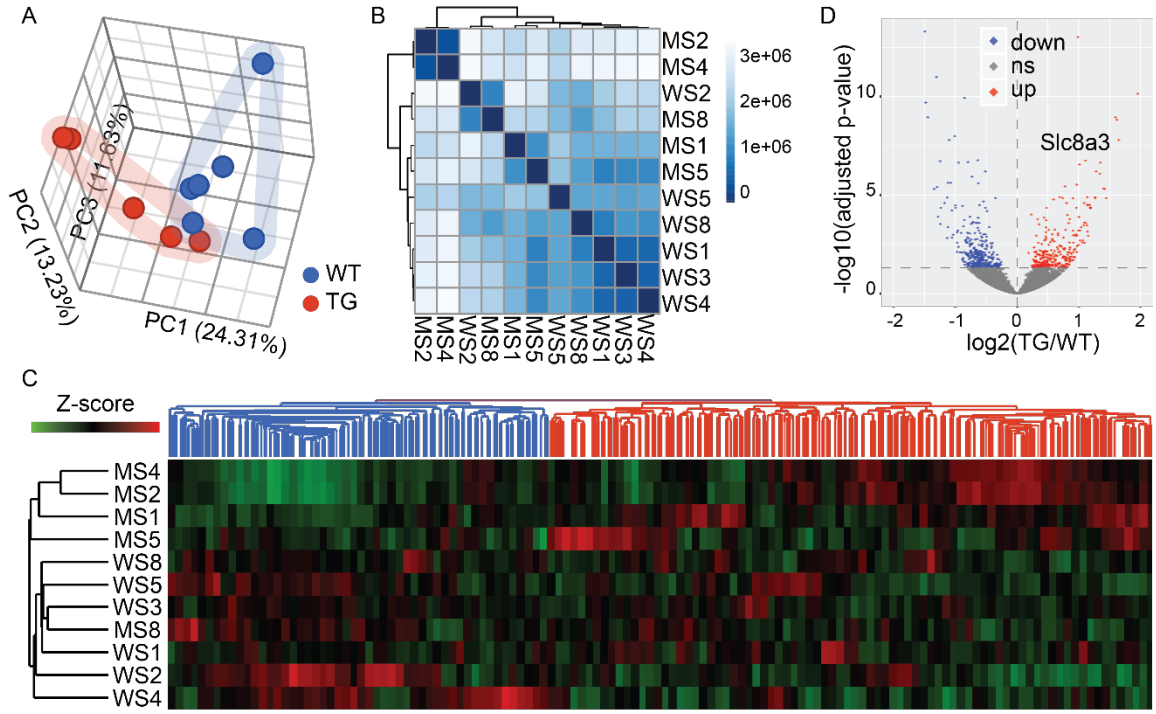


**Figure1. Conduction of RNA sequencing on samples of TGAC8 vs. WT mouse SAN.** **A-C**. PCA (A), Sample distance matrix (B), and hierarchial cluster (C) of all samples used in the TGAC8 SAN transcriptome (WT: WS1, WS2, WS3, WS4, WS5, WS8; TGAC8: MS1, MS2, MS4, MS5, MS8). **D**. Volcano plot of TGAC8 SAN RNA-seq data. Genes with adjusted p-value less than 0.05 are regarded as significantly regulated by the overexpression of AC8, among which genes with log2(TG/WT) more than zero and less than zero are marked as red (up) and blue dots (down) respectively. Other genes are nonsignificantly regulated and marked as grey dots (ns). One of the most significantly upregulated genes, Slc8a3, is labeled besides its dot.

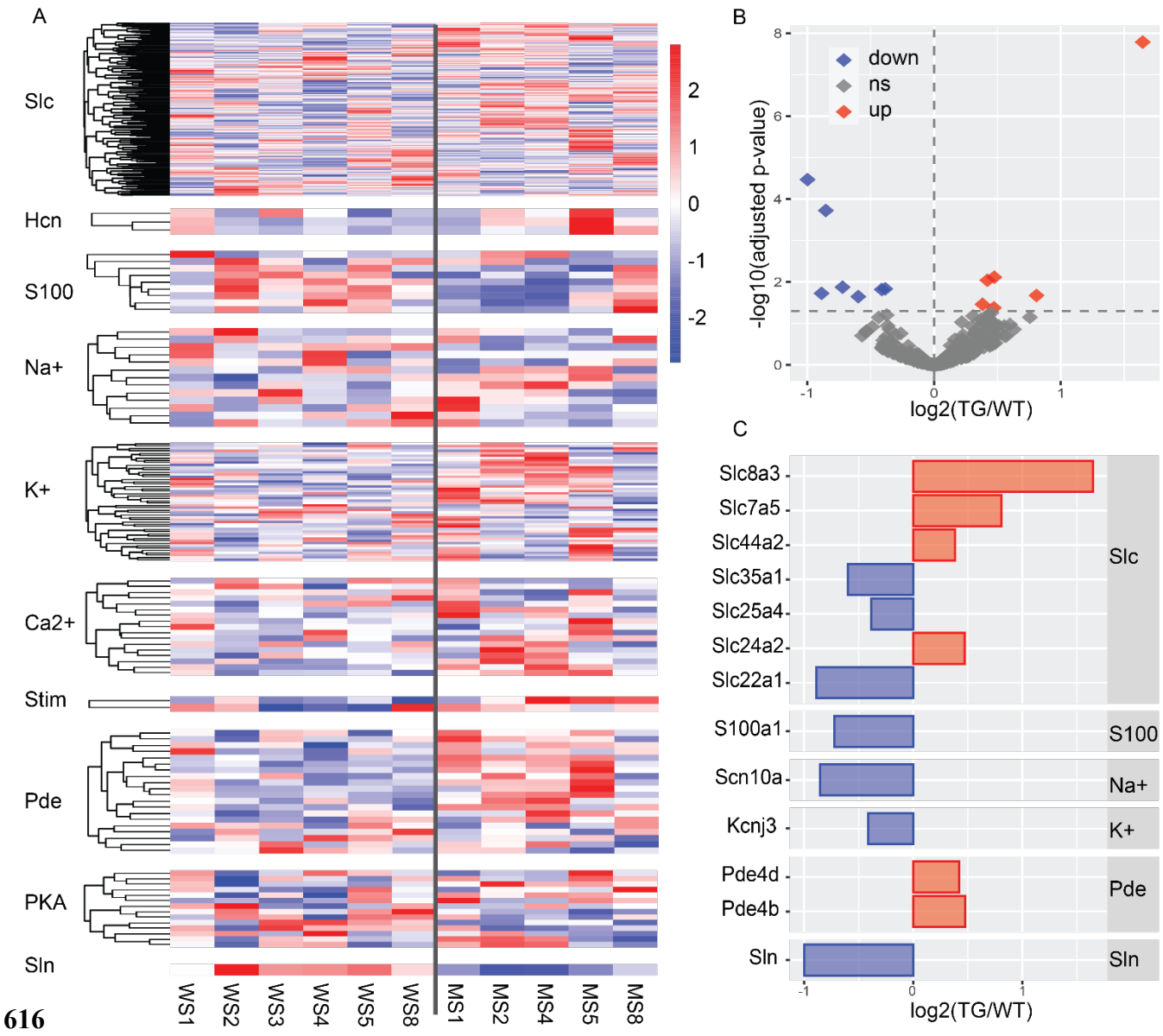


**Figure 2. Marker genes in TGAC8 SAN transcriptome. A**. Heatmap of selected families of genes related to ion channels and AC8-cAMP-PKA pathway. **B**. Volcano plot of all selected genes in A. Red dots represent upregulated genes (adjusted p-value < 0.05 and log2FoldChange > 0); blue dots represent downregulated genes (adjusted p-value < 0.05 and log2FoldChange < 0); grey dots represent nonsignificantly regulated genes (adjusted p-value ≥ 0.05). **C**. Bar plot of expressions of genes that are significantly regulated in AC8 SAN (up and down).

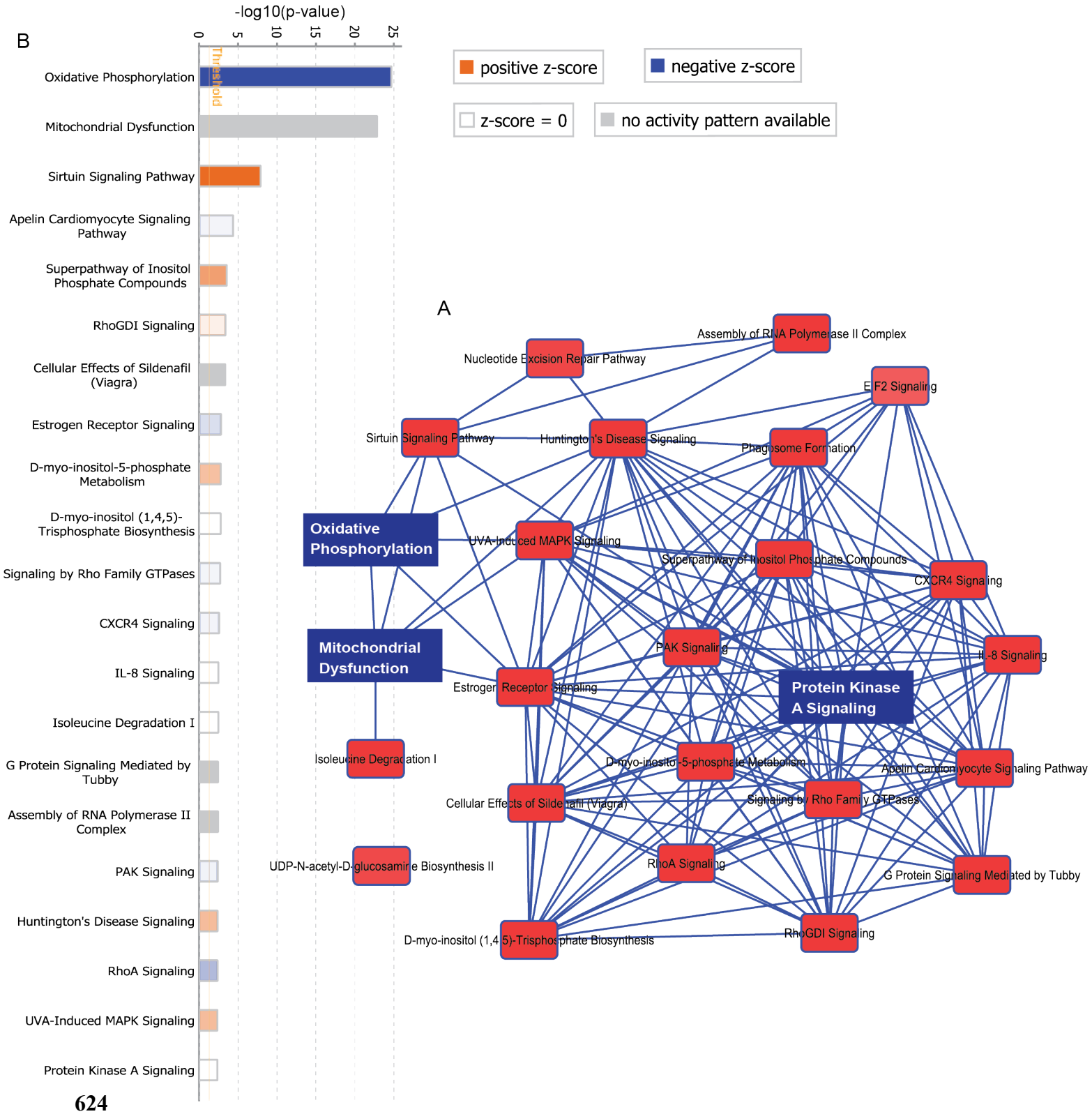
B
-log10(p-value)
0
5
10
15
20
25
Threshold
Oxidative Phosphorylation
Mitochondrial Dysfunction
Sirtuin Signaling Pathway
Apelin Cardiomyocyte Signaling Pathway
Superpathway of Inositol Phosphate Compounds
RhoGDI Signaling
Cellular Effects of Sildenafil (Viagra)
Estrogen Receptor Signaling
D-myo-inositol-5-phosphate Metabolism
D-myo-inositol (1,4,5)-Trisphosphate Biosynthesis
Signaling by Rho Family GTPases
CXCR4 Signaling
IL-8 Signaling
Isoleucine Degradation I
G Protein Signaling Mediated by Tubby
Assembly of RNA Polymerase II Complex
PAK Signaling
Huntington's Disease Signaling
RhoA Signaling
UVA-Induced MAPK Signaling
Protein Kinase A Signaling
positive z-score
negative z-score
z-score = 0
no activity pattern available
A
Assembly of RNA Polymerase II Complex
Nucleotide Excision Repair Pathway
EIF2 Signaling
Sirtuin Signaling Pathway
Huntington's Disease Signaling
Phagosome Formation
Oxidative Phosphorylation
UVA-Induced MAPK Signaling
Superpathway of Inositol Phosphate Compounds
CXCR4 Signaling
Mitochondrial Dysfunction
PAK Signaling
IL-8 Signaling
Estrogen Receptor Signaling
Protein Kinase A Signaling
Isoleucine Degradation I
D-myo-inositol-5-phosphate Metabolism
Apelin Cardiomyocyte Signaling Pathway
Cellular Effects of Sildenafil (Viagra)
Signaling by Rho Family GTPases
UDP-N-acetyl-D-glucosamine Biosynthesis II
RhoA Signaling
G Protein Signaling Mediated by Tubby
D-myo-inositol (1,4,5)-Trisphosphate Biosynthesis
RhoGDI Signaling

624

625 **Figure 3. Ingenuity Pathway Analysis of TGAC8 SAN transcriptome. A**. Overlapping
626 network of top 25 pathways. Three representative pathways, Oxidative Phosphorylation,
627 Mitochondrial Dysfunction, and Protein Kinase A Signaling, are marked in blue
628 rectangles. **B**. Top 21 canonical pathways enriched in IPA, ranked by -log10(p-value).
629 The 20$^{th}$ and 21$^{st}$ pathways have the same -log10(p-value). Bar color indicates activation
630 state based on the uploaded transcriptome into IPA. Orange bars with positive z-scores
631 and blue bars with negative z-scores denote activated and inhibited pathways
632 respectively. The darker the more significant. White bars denote pathways insignificantly
633 activated or inhibited with z-score equal to zero. Grey bars denote pathways for which no
634 activity pattern is available within IPA knowledgebase.

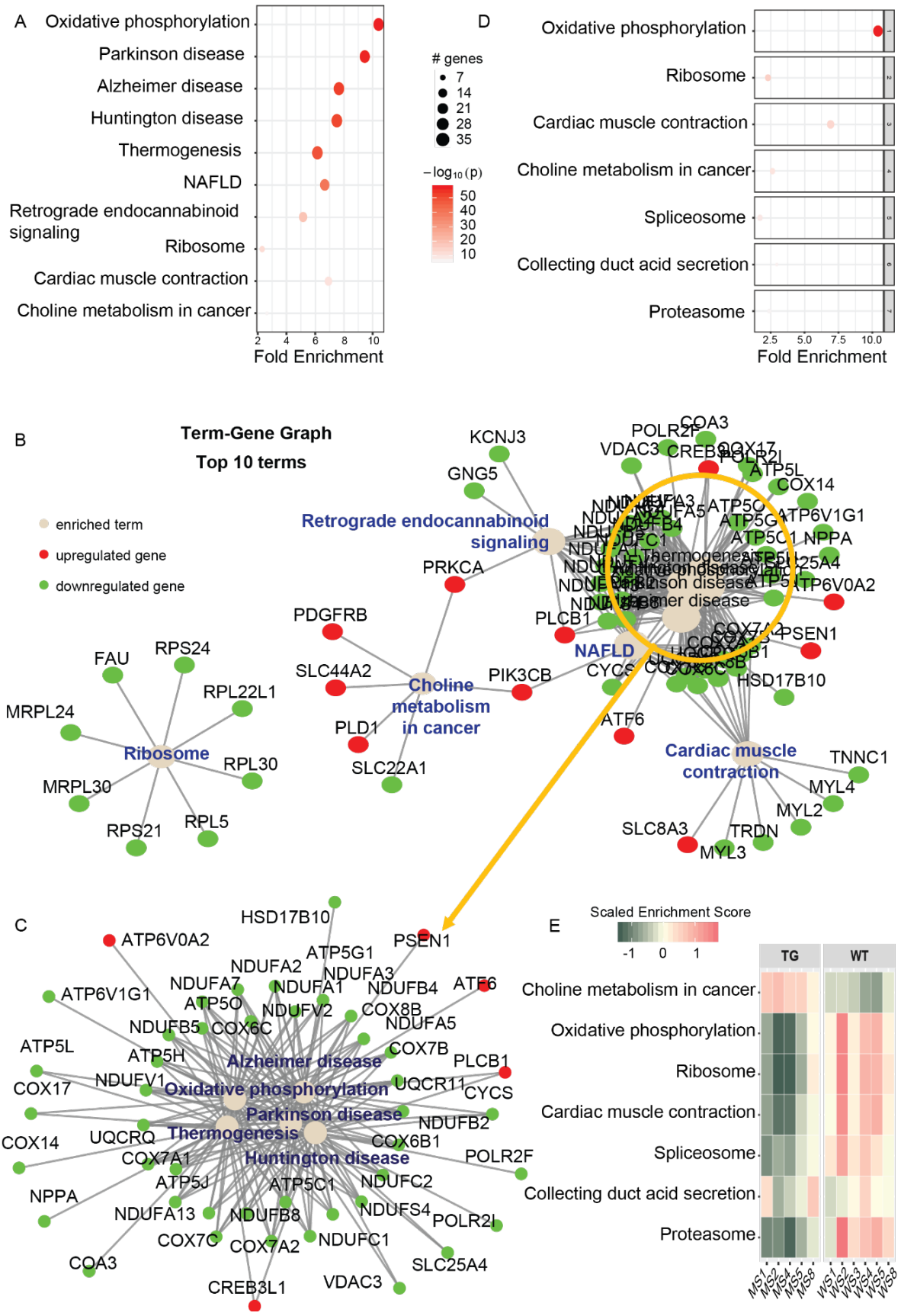
A
Oxidative phosphorylation
Parkinson disease
Alzheimer disease
Huntington disease
Thermogenesis
NAFLD
Retrograde endocannabinoid signaling
Ribosome
Cardiac muscle contraction
Choline metabolism in cancer
Fold Enrichment
# genes
7
14
21
28
35
−log10(p)
50
40
30
20
10
D
Oxidative phosphorylation
Ribosome
Cardiac muscle contraction
Choline metabolism in cancer
Spliceosome
Collecting duct acid secretion
Proteasome
Fold Enrichment
B
Term-Gene Graph
Top 10 terms
enriched term
upregulated gene
downregulated gene
Retrograde endocannabinoid signaling
Choline metabolism in cancer
NAFLD
Ribosome
Cardiac muscle contraction
C
Alzheimer disease
Oxidative phosphorylation
Parkinson disease
Thermogenesis
Huntington disease
E
Scaled Enrichment Score
TG
WT
Choline metabolism in cancer
Oxidative phosphorylation
Ribosome
Cardiac muscle contraction
Spliceosome
Collecting duct acid secretion
Proteasome

635

636 **Figure 4. KEGG pathway clustering analysis of TGAC8 SAN transcriptome. A**.
637 Bubble graph of KEGG pathway analysis of TGAC8 SAN transcriptome. X-axis is fold
638 enrichment of pathway, bubble size represents number of genes in a pathway, and bubble
639 color gradient indicates significance with -log10(p-value). **B**. Term-gene graph of top 10
640 terms, ranked by fold enrichment. Grey dot denotes enriched term. Red and green dots
641 denote upregulated and downregulated genes respectively. Some genes are enriched in
642 more than one pathway. The pathways on the top right are aggregated and thus zoomed in
643 as Figure **C**. **D**. Bubble graph of hub KEGG pathways in each pathway cluster using
644 pathfindR package. Legend same to Figure A. **E**. Heat map of term score in each sample.
645 Color gradient indicates scaled enrichment score. The more red, the more enriched.

A

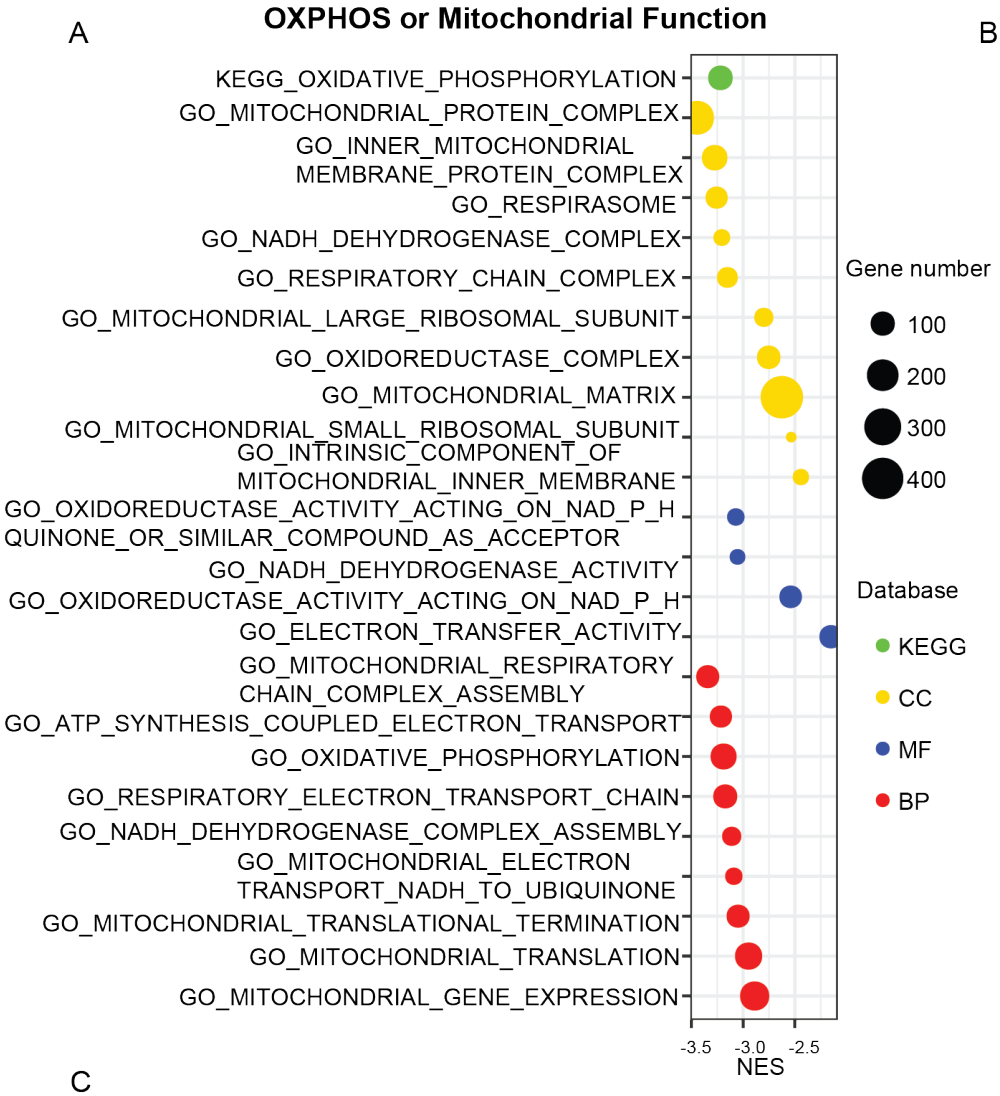
OXPHOS or Mitochondrial Function
KEGG_OXIDATIVE_PHOSPHORYLATION
GO_MITOCHONDRIAL_PROTEIN_COMPLEX
GO_INNER_MITOCHONDRIAL MEMBRANE_PROTEIN_COMPLEX
GO_RESPIRASOME
GO_NADH_DEHYDROGENASE_COMPLEX
GO_RESPIRATORY_CHAIN_COMPLEX
GO_MITOCHONDRIAL_LARGE_RIBOSOMAL_SUBUNIT
GO_OXIDOREDUCTASE_COMPLEX
GO_MITOCHONDRIAL_MATRIX
GO_MITOCHONDRIAL_SMALL_RIBOSOMAL_SUBUNIT
GO_INTRINSIC_COMPONENT_OF MITOCHONDRIAL_INNER_MEMBRANE
GO_OXIDOREDUCTASE_ACTIVITY_ACTING_ON_NAD_P_H QUINONE_OR_SIMILAR_COMPOUND_AS_ACCEPTOR
GO_NADH_DEHYDROGENASE_ACTIVITY
GO_OXIDOREDUCTASE_ACTIVITY_ACTING_ON_NAD_P_H
GO_ELECTRON_TRANSFER_ACTIVITY
GO_MITOCHONDRIAL_RESPIRATORY CHAIN_COMPLEX_ASSEMBLY
GO_ATP_SYNTHESIS_COUPLED_ELECTRON_TRANSPORT
GO_OXIDATIVE_PHOSPHORYLATION
GO_RESPIRATORY_ELECTRON_TRANSPORT_CHAIN
GO_NADH_DEHYDROGENASE_COMPLEX_ASSEMBLY
GO_MITOCHONDRIAL_ELECTRON TRANSPORT_NADH_TO_UBIQUINONE
GO_MITOCHONDRIAL_TRANSLATIONAL_TERMINATION
GO_MITOCHONDRIAL_TRANSLATION
GO_MITOCHONDRIAL_GENE_EXPRESSION
-3.5
-3.0
-2.5
NES
Gene number
100
200
300
400
Database
KEGG
CC
MF
BP

B

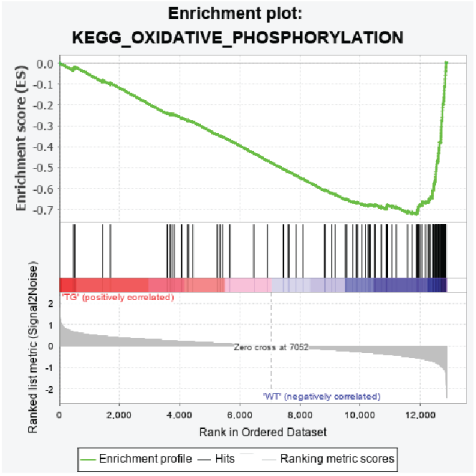
Enrichment plot:
KEGG_OXIDATIVE_PHOSPHORYLATION
Enrichment score (ES)
Ranked list metric (Signal2Noise)
'TG' (positively correlated)
Zero cross at 7052
'WT' (negatively correlated)
Rank in Ordered Dataset
Enrichment profile
Hits
Ranking metric scores

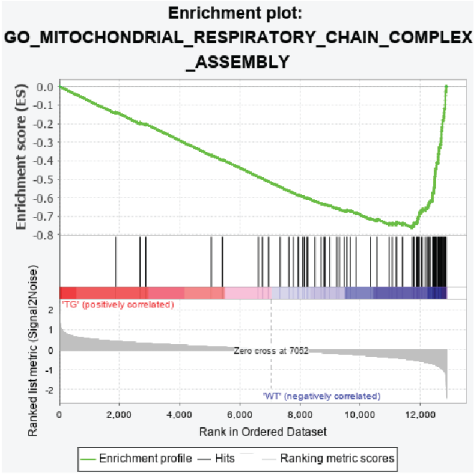
Enrichment plot:
GO_MITOCHONDRIAL_RESPIRATORY_CHAIN_COMPLEX_ASSEMBLY
Enrichment score (ES)
Ranked list metric (Signal2Noise)
'TG' (positively correlated)
Zero cross at 7052
'WT' (negatively correlated)
Rank in Ordered Dataset
Enrichment profile
Hits
Ranking metric scores

C

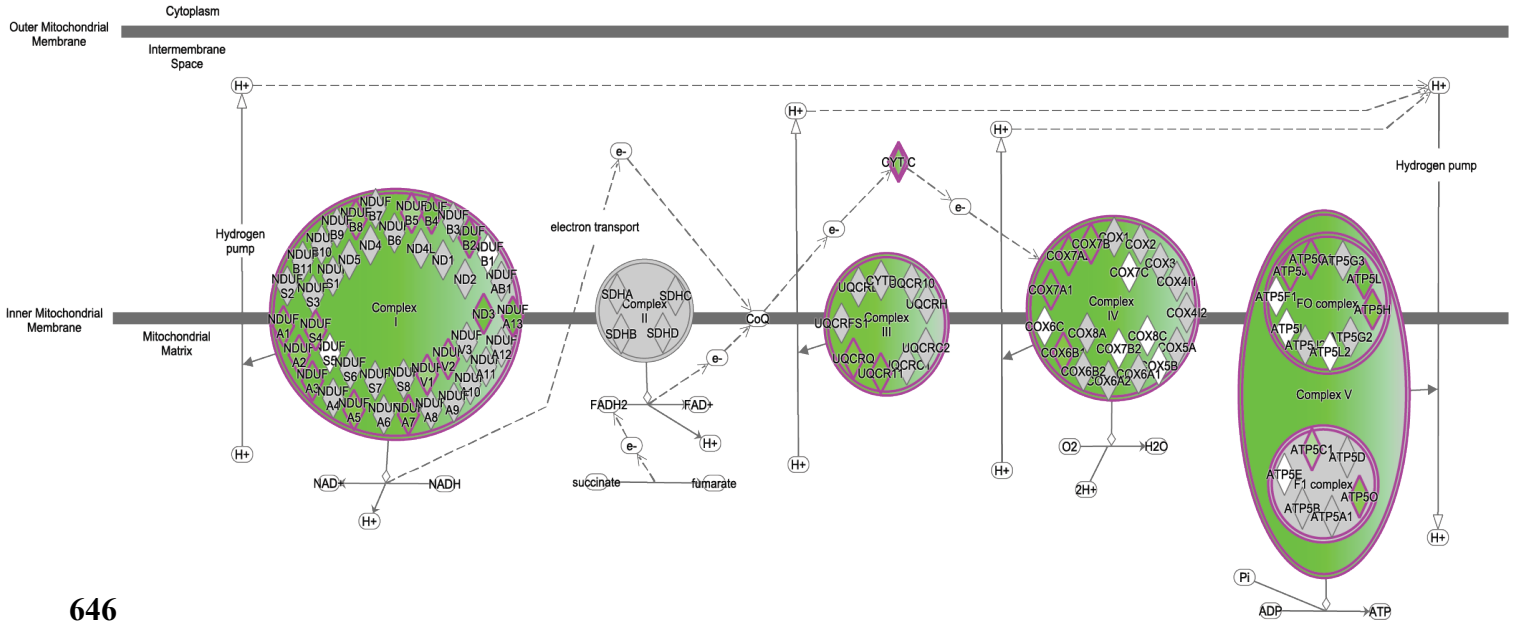
Cytoplasm
Outer Mitochondrial Membrane
Intermembrane Space
Inner Mitochondrial Membrane
Mitochondrial Matrix
Hydrogen pump
Hydrogen pump
electron transport
Complex I
Complex II
Complex III
Complex IV
Complex V
F1 complex
FO complex
CoQ
CYT C
NAD+
NADH
FADH2
FAD+
succinate
fumarate
O2
H2O
2H+
Pi
ADP
ATP

**Figure 5. Downregulated mitochondria and mitochondrial functions in TGAC8 SAN. A**. Bubble graph of GSEA of TGAC8 SAN transcriptome. X-axis is normalized enrichment score (NES) in GSEA, bubble size represents number of genes in a term, and bubble color indicates enrichment using four different databases (KEGG, GO_CC, GO_MF, GO_BP). **B**. Two representative GSEA enrichment plots. Top: enriched using KEGG database; bottom: GO_BP. **C**. Visualization of changed genes in the term of oxidative phosphorylation, generated in IPA. Genes with purple outline are changed significantly. All genes are in green, indicating decreased.

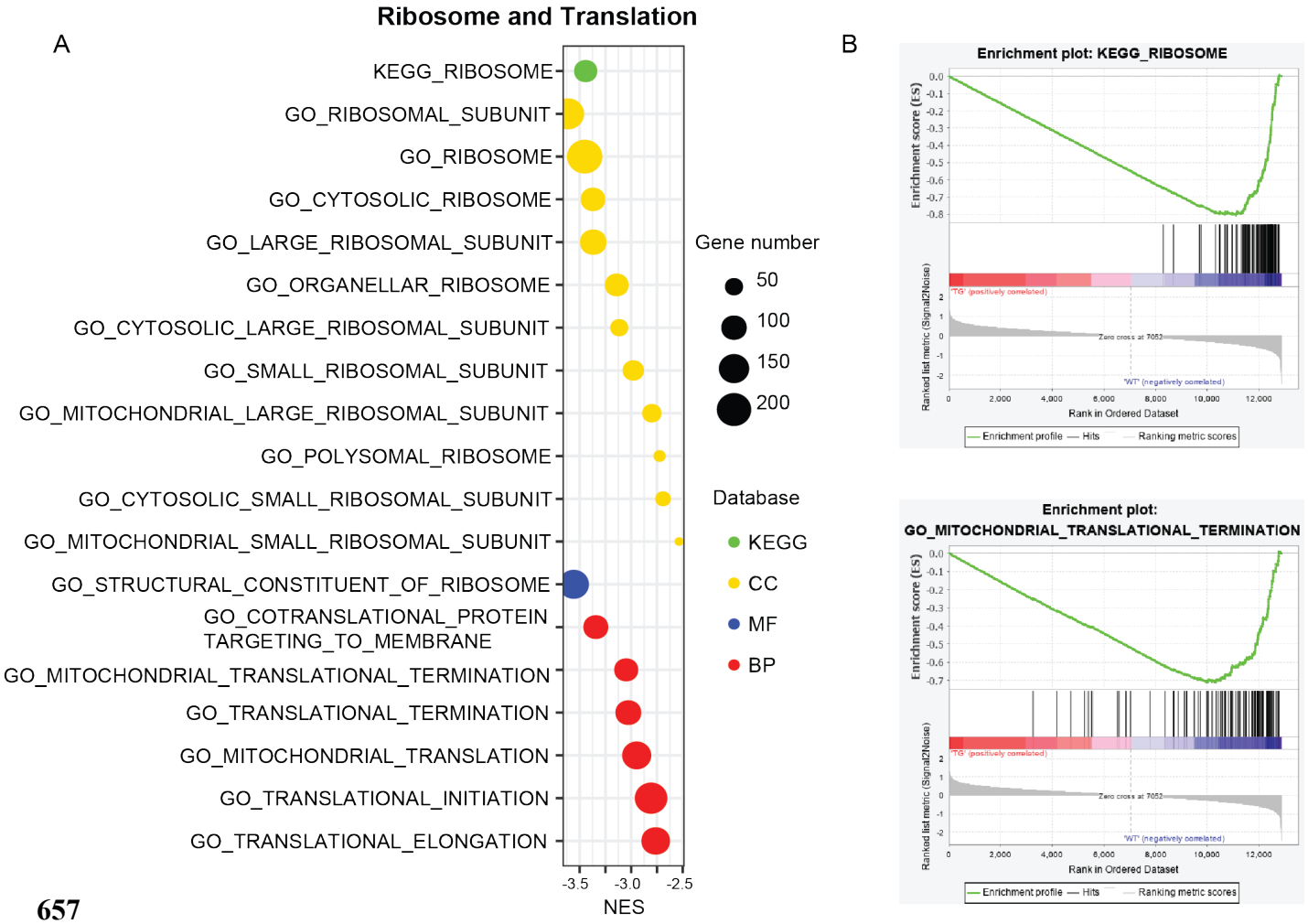


**Figure 6. Downregulated ribosome and translation in TGAC8 SAN. A**. Bubble graph of GSEA of TGAC8 SAN transcriptome. X-axis is normalized enrichment score (NES) in GSEA, bubble size represents number of genes in a term, and bubble color indicates enrichment using four different databases (KEGG, GO_CC, GO_MF, GO_BP). **B**. Two representative GSEA enrichment plots. Top: enriched using KEGG database; bottom: GO_BP.

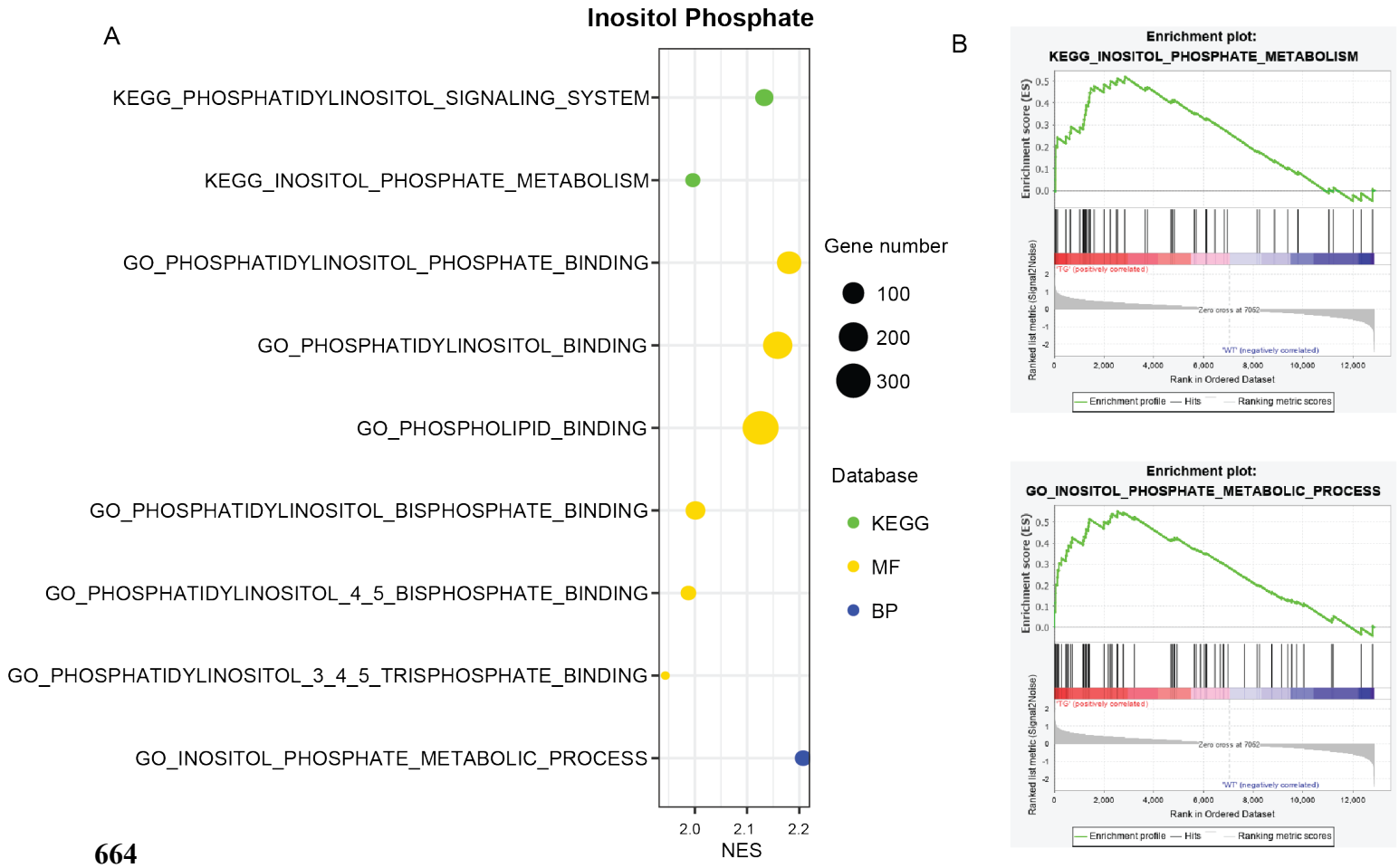


**Figure 7. Upregulated inositol phosphate and its metabolism in TGAC8 SAN. A**. Bubble graph of GSEA of TGAC8 SAN transcriptome. X-axis is normalized enrichment score (NES) in GSEA, bubble size represents number of genes in a term, and bubble color indicates enrichment using four different databases (KEGG, GO_CC, GO_MF, GO_BP). **B**. Two representative GSEA enrichment plots. Top: enriched using KEGG database; bottom: GO_BP.

A

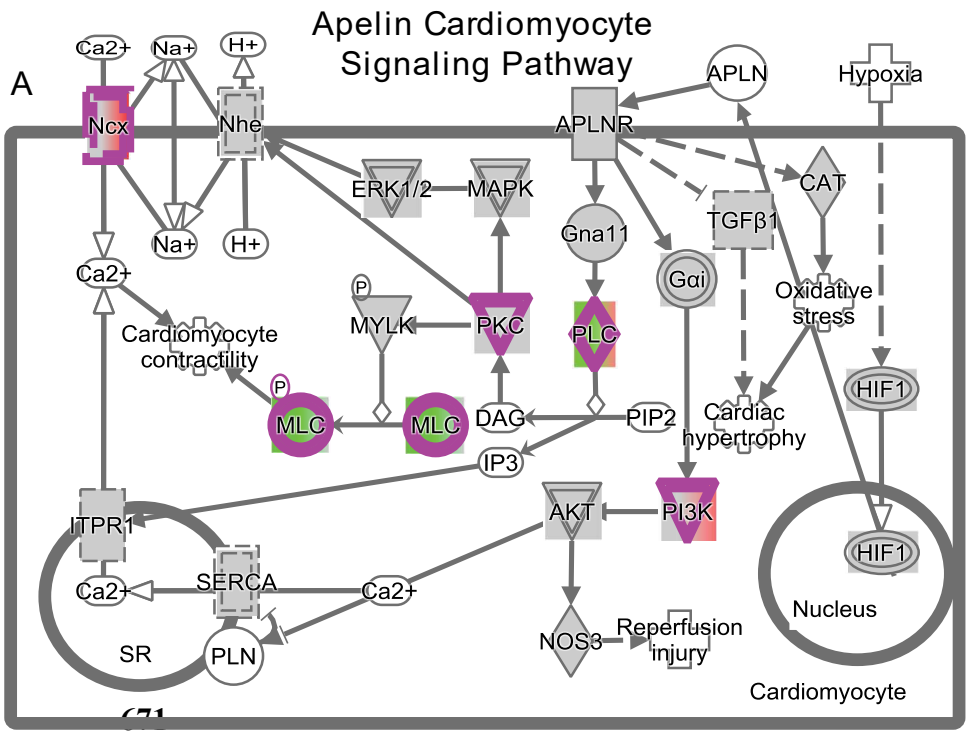
Apelin Cardiomyocyte
Signaling Pathway
Ca2+
Na+
H+
Ncx
Nhe
APLN
Hypoxia
APLNR
ERK1/2
MAPK
CAT
Gna11
TGFβ1
Na+
H+
Ca2+
Gαi
Oxidative
stress
P
MYLK
PKC
PLC
Cardiomyocyte
contractility
P
MLC
MLC
DAG
PIP2
Cardiac
hypertrophy
HIF1
IP3
AKT
PI3K
ITPR1
HIF1
Ca2+
SERCA
Ca2+
Nucleus
NOS3
Reperfusion
injury
SR
PLN
Cardiomyocyte

B

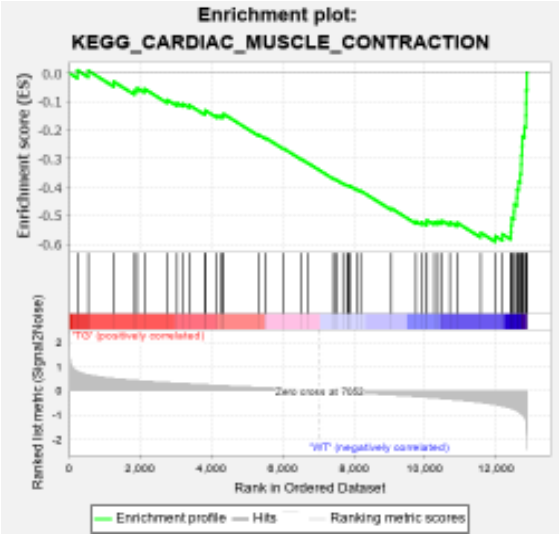
Enrichment plot:
KEGG_CARDIAC_MUSCLE_CONTRACTION
Enrichment score (ES)
0.0
-0.1
-0.2
-0.3
-0.4
-0.5
-0.6
"TG" (positively correlated)
Zero cross at 7052
"WT" (negatively correlated)
Ranked list metric (Signal2Noise)
2
1
0
-1
-2
0
2,000
4,000
6,000
8,000
10,000
12,000
Rank in Ordered Dataset
Enrichment profile
Hits
Ranking metric scores

C

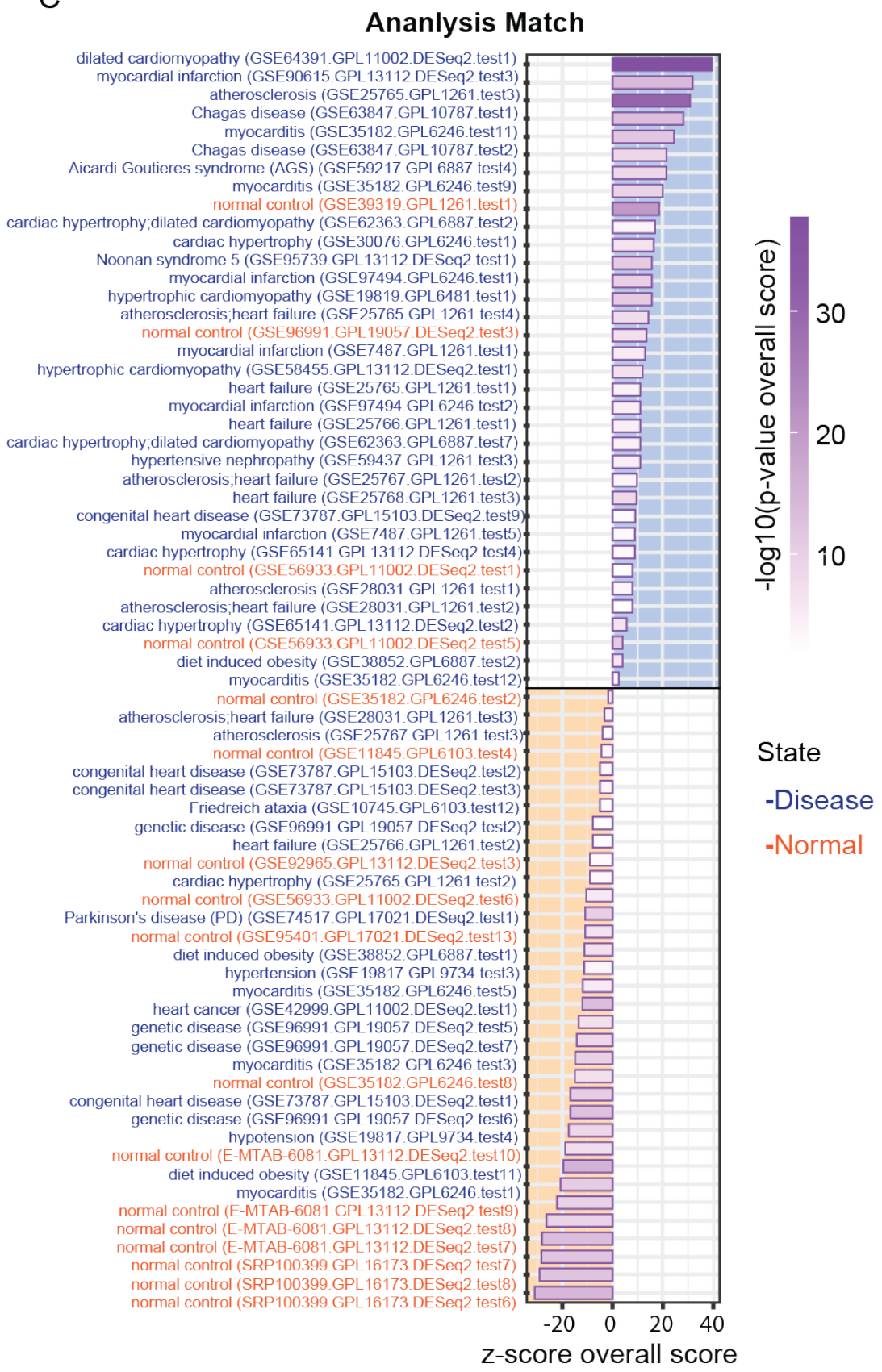
Ananlysis Match
dilated cardiomyopathy (GSE64391.GPL11002.DESeq2.test1)
myocardial infarction (GSE90615.GPL13112.DESeq2.test3)
atherosclerosis (GSE25765.GPL1261.test3)
Chagas disease (GSE63847.GPL10787.test1)
myocarditis (GSE35182.GPL6246.test11)
Chagas disease (GSE63847.GPL10787.test2)
Aicardi Goutieres syndrome (AGS) (GSE59217.GPL6887.test4)
myocarditis (GSE35182.GPL6246.test9)
normal control (GSE39319.GPL1261.test1)
cardiac hypertrophy;dilated cardiomyopathy (GSE62363.GPL6887.test2)
cardiac hypertrophy (GSE30076.GPL6246.test1)
Noonan syndrome 5 (GSE95739.GPL13112.DESeq2.test1)
myocardial infarction (GSE97494.GPL6246.test1)
hypertrophic cardiomyopathy (GSE19819.GPL6481.test1)
atherosclerosis;heart failure (GSE25765.GPL1261.test4)
normal control (GSE96991.GPL19057.DESeq2.test3)
myocardial infarction (GSE7487.GPL1261.test1)
hypertrophic cardiomyopathy (GSE58455.GPL13112.DESeq2.test1)
heart failure (GSE25765.GPL1261.test1)
myocardial infarction (GSE97494.GPL6246.test2)
heart failure (GSE25766.GPL1261.test1)
cardiac hypertrophy;dilated cardiomyopathy (GSE62363.GPL6887.test7)
hypertensive nephropathy (GSE59437.GPL1261.test3)
atherosclerosis;heart failure (GSE25767.GPL1261.test2)
heart failure (GSE25768.GPL1261.test3)
congenital heart disease (GSE73787.GPL15103.DESeq2.test9)
myocardial infarction (GSE7487.GPL1261.test5)
cardiac hypertrophy (GSE65141.GPL13112.DESeq2.test4)
normal control (GSE56933.GPL11002.DESeq2.test1)
atherosclerosis (GSE28031.GPL1261.test1)
atherosclerosis;heart failure (GSE28031.GPL1261.test2)
cardiac hypertrophy (GSE65141.GPL13112.DESeq2.test2)
normal control (GSE56933.GPL11002.DESeq2.test5)
diet induced obesity (GSE38852.GPL6887.test2)
myocarditis (GSE35182.GPL6246.test12)
normal control (GSE35182.GPL6246.test2)
atherosclerosis;heart failure (GSE28031.GPL1261.test3)
atherosclerosis (GSE25767.GPL1261.test3)
normal control (GSE11845.GPL6103.test4)
congenital heart disease (GSE73787.GPL15103.DESeq2.test2)
congenital heart disease (GSE73787.GPL15103.DESeq2.test3)
Friedreich ataxia (GSE10745.GPL6103.test12)
genetic disease (GSE96991.GPL19057.DESeq2.test2)
heart failure (GSE25766.GPL1261.test2)
normal control (GSE92965.GPL13112.DESeq2.test3)
cardiac hypertrophy (GSE25765.GPL1261.test2)
normal control (GSE56933.GPL11002.DESeq2.test6)
Parkinson's disease (PD) (GSE74517.GPL17021.DESeq2.test1)
normal control (GSE95401.GPL17021.DESeq2.test13)
diet induced obesity (GSE38852.GPL6887.test1)
hypertension (GSE19817.GPL9734.test3)
myocarditis (GSE35182.GPL6246.test5)
heart cancer (GSE42999.GPL11002.DESeq2.test1)
genetic disease (GSE96991.GPL19057.DESeq2.test5)
genetic disease (GSE96991.GPL19057.DESeq2.test7)
myocarditis (GSE35182.GPL6246.test3)
normal control (GSE35182.GPL6246.test8)
congenital heart disease (GSE73787.GPL15103.DESeq2.test1)
genetic disease (GSE96991.GPL19057.DESeq2.test6)
hypotension (GSE19817.GPL9734.test4)
normal control (E-MTAB-6081.GPL13112.DESeq2.test10)
diet induced obesity (GSE11845.GPL6103.test11)
myocarditis (GSE35182.GPL6246.test1)
normal control (E-MTAB-6081.GPL13112.DESeq2.test9)
normal control (E-MTAB-6081.GPL13112.DESeq2.test8)
normal control (E-MTAB-6081.GPL13112.DESeq2.test7)
normal control (SRP100399.GPL16173.DESeq2.test7)
normal control (SRP100399.GPL16173.DESeq2.test8)
normal control (SRP100399.GPL16173.DESeq2.test6)
-20
0
20
40
z-score overall score
-log10(p-value overall score)
30
20
10
State
-Disease
-Normal

672

673 **Figure 8. Association with impaired cardiac functions in TGAC8 SAN. A**.

674 Visualization of changed genes in the term of apelin cardiomyocyte signaling pathway,

675 generated in IPA. Genes with purple outline are changed significantly. Green represents

676 downregulated, and red represents upregulated. **B**. GSEA enrichment plot of cardiac

677 muscle contraction. **C**. Bar plot of analysis match with public projects in IPA. X-axis is z-

678 score overall score. Positive and negative scores indicate positive and negative

679 correlations respectively. Color gradient represents -log10(p-value overall score),

680 indicating the confidence of the analysis match. The darker, the high confidence. Y-axis is

681 public project's name. Blue indicates disease state, and red indicates normal state.

Figure 9

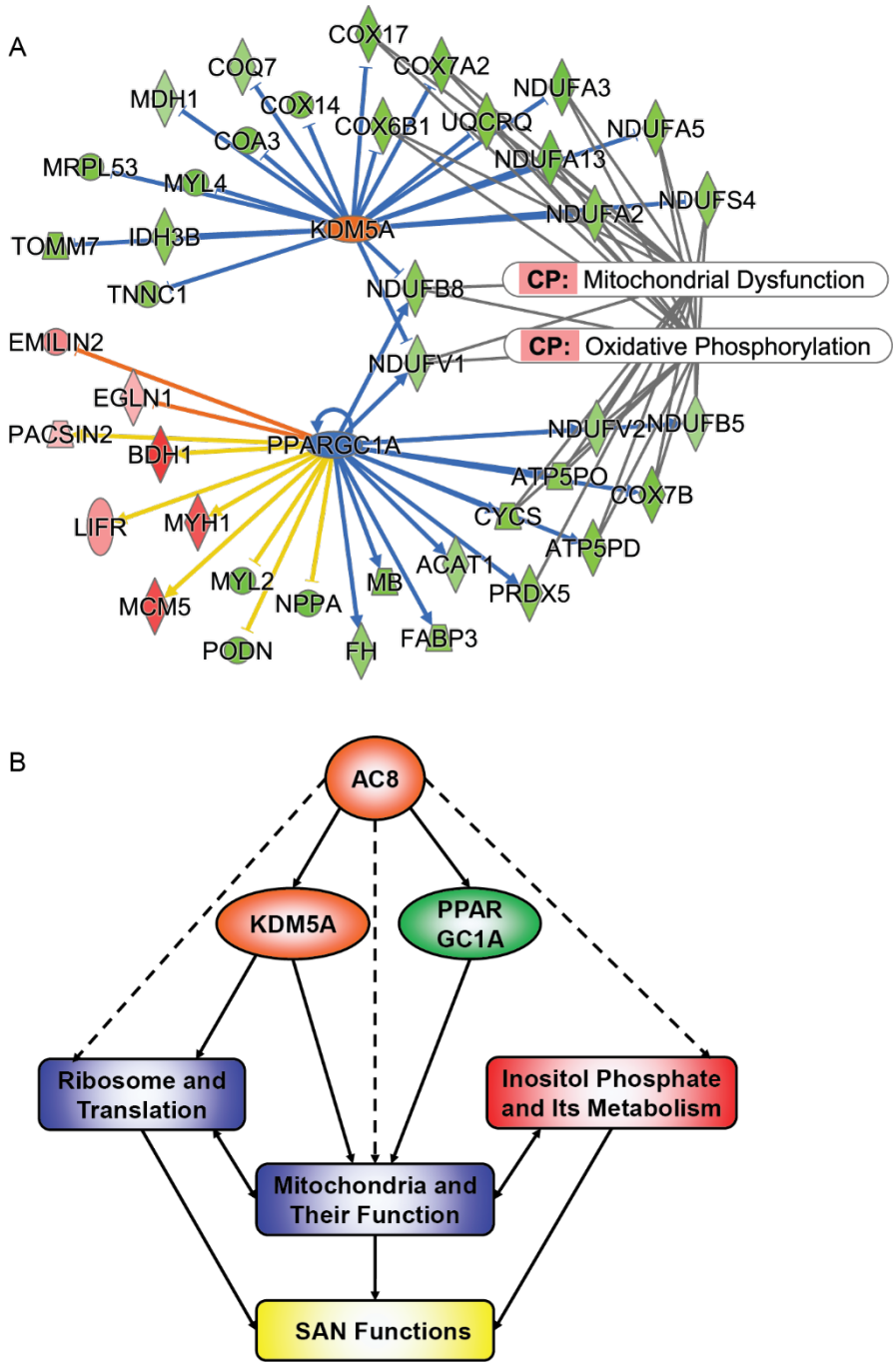


682

683 **Figure 9. Regulatory pathway of TGAC8 SAN transcriptome. A**. Mechanistic

684 pathway from predicted upstream regulators to regulated downstream pathways. Two

685 oval dots in the center denote the upstream regulators predicted on the basis of TGAC8

686 SAN transcriptome. Blue indicates inhibited, and orange indicates activated. Surrounding

687 dots denote genes that are under the control of the two upstream regulators and changed
688 significantly in TGAC8 SAN transcriptome. Green indicates downregulation, and red
689 indicates upregulation. Edges between dots represent relationships between genes.
690 Arrows denotes promotion, and short bar denotes suppression. Blue and orange edges
691 indicate that the predicted activation state of upstream regulator leads to the gene
692 downregulation and upregulation respectively in TGAC8 SAN transcriptome. Yellow
693 edges represent findings inconsistent with state of downstream molecule. Two text boxes
694 on the right represent downstream pathways that are enriched from differentially
695 expressed genes. **B**. Deduced schematic: Transgenic overexpression of AC8 in SAN
696 suppresses ribosome and translation, and mitochondria and their functions, while
697 promotes inositol phosphate and its metabolism, thus associated with impaired SAN
698 functions. Two transcription regulators, KDM5A and PPARGC1A, are possible mediators
699 of overexpression of AC8.

700